Intruder friction effects on granular impact dynamics

Hu Zheng,[1,2,*] Dong Wang,[2] David Z. Chen,[2] Meimei Wang,[2,3] and Robert P. Behringer[2]
[1]*School of Earth Science and Engineering, Hohai University, Nanjing, Jiangsu 211100, China*
[2]*Department of Physics & Center for Nonlinear and Complex Systems, Duke University, Durham, North Carolina 27708, USA*
[3]*School of Civil and Resource Engineering, University of Science and Technology Beijing, Beijing 100083, China*

(Received 7 April 2018; published 17 September 2018)

There is considerable recent interest in intruders impacting into granular materials. Many studies focus on a collisional model where the drag force acting on an intruder varies as the square of the intruder speed. However, it is unclear how intruder friction affects granular impact dynamics. Here, we experimentally study impacts into quasi-two-dimensional beds of photoelastic granular beds of three circular intruders of similar size and mass, but with varying friction coefficients associated with the intruder edges (smooth, "sandy," and gear). We compare typical measures of the dynamics for the three intruders, including impact depth and speed vs time. We show that the smooth and sandy intruders share similar impact dynamics, while the gear intruder displays smaller impact depth, speed, and impact time. We attribute the differences between the gear intruder's dynamics and those of the other two to differences in the collision-generated force networks associated with the grain-scale roughness of the gear intruder. For the smooth and sandy intruders, the force networks align close to the normal direction of the intruder boundaries. For the gear intruder, the grain-scale geometric roughness leads to force chains that are closer to vertical, rather than in the coarse-grained normal direction to the intruder edge. This leads to a stronger drag force for the gear intruder. Hence, in the range that we have explored, the granular impact dynamics are highly sensitive to grain-scale roughness of the intruder and relatively insensitive to microscale roughness that is associated with the conventional friction coefficient.

DOI: 10.1103/PhysRevE.98.032904

I. INTRODUCTION

Intruder impact into granular media has wide applications such as soil penetration tests and ballistics, and has attracted significant scientific attention in recent years [1–10]. Typical impact experiments drop or push an intruder into a granular bed and analyze the microscale movement [8–11] of the grains and/or the intruder dynamics [12–14]. A classical empirical model that has been widely used to characterize the average dynamics of the intruder trajectories during vertical impacts into grains has the following form:

$$m\frac{d\dot{z}}{dt} = \frac{dK}{dz} = mg - f(z) - \frac{2h(z)}{m}K, \qquad (1)$$

where z is the intruder depth relative to the top of the granular surface, K is the kinetic energy of the intruder, $K = \frac{1}{2}m\dot{z}^2$, m is the intruder mass, g is the gravitational acceleration, $f(z)$ characterizes static effects, and is often assumed to be linear in z, $f(z) = f_0 + kz$, and $h(z)$ is often assumed to be constant.

The last term on the right side of Eq. (1) denotes the collisional momentum transfer between the intruder and the grains. Recently, Clark *et al.* [5–7] showed that Eq. (1) captures the slow (average) dynamics, but that the force networks generated along the intruder-granular interface fluctuate rapidly in space and time. They constructed a collisional model that explicitly invokes collisions between the intruder and clusterlike segments of the force network to derive the velocity-squared drag force [7]. Their collisional model captures the dynamics of intruder deceleration and small amounts of rotation, and has been applied in wet granular impact studies [15,16], and extended to three-dimensional impact dynamics [17]. This model is derived based on an assumption that force chains are oriented in the normal direction at the intruder boundary, as observed in the experiments. Consequently, friction between intruder and particles is not included in this model, and is not needed to describe the experimental results of Clark *et al.* [5–7] and Bester *et al.* [17]. An immediate question is then, does intruder friction affect impact dynamics, and if so how?

In this paper, we report the dependence of intruder dynamics on the friction between the intruder surface and the granular material during impacts into two-dimensional photoelastic granular beds. We vary the intruders' friction by changing the edge properties of the intruders from smooth to rough at the grain scale. For three different intruders, we consider data for the intruder speed, the nature of the force chains that are excited at the intruder interface, and the final penetration depth. The basic principles of the experimental techniques are similar to those described in Clark *et al.* [5–7,18]. In addition to what has been done previously, we analyze in detail the direction of the force chains created during impact relative to the intruder normal. The distribution of these directions for the roughest intruder differ substantially from the distributions for the other two intruders, and point to an explanation for differences in drag forces.

II. EXPERIMENTAL PROTOCOLS

The experimental apparatus consists of two Plexiglas sheets (0.91 m × 1.22 m × 1.25 cm) separated by a thin gap

*hz64@phy.duke.edu

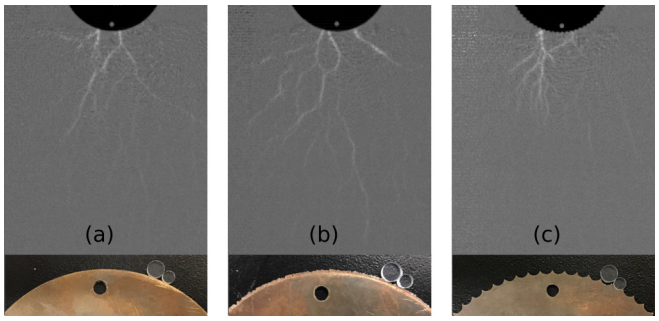

FIG. 1. Snapshots of force propagation in the granular bed after impact with $v_0 \approx 2.2$ m/s. (a) Bronze intruder with a relatively smooth boundary. (b) "Sandy" intruder coated with 1-mm-diameter sand, which has a large conventional friction coefficient. (c) Gear intruder, showing the nature of the grain-scale geometric friction.

(3.3 mm) filled with disks (3 mm thick) of two different diameters (6 and 4.3 mm) to avoid crystallization [18]. The disks are photoelastic with elastic modulus of 2.5 GPa and Poisson's ratio of 0.38, custom made from polyurethane sheets (Vishay PSM-1). Intruders are disks machined from bronze sheet (bulk density of 8.91 g/cm^3 and thickness of 0.23 cm). We varied the intruder-granular friction by making three different discs with boundaries that are respectively smooth, coated with sand (average sand grain diameter is $\sim$1 mm), and machined to have a gear profile. Figure 1 shows a portion of the edge of each intruder. The smooth intruder has relatively low friction coefficient, $\mu = 0.37$. The sand coated intruder has a relatively high friction coefficient, $\mu = 1.51$. The gear intruder has large "geometric friction" in addition to material friction. In simulations of static packings, geometrical asperities have been used as an effective way to impart frictional interactions between particles that otherwise have a zero friction coefficient [19]. The size of smooth and gear intruders are both 96 mm, and the diameter of the sand-coated intruder is 98 mm. The weights are 149.78, 150.32, and 148.11 g, corresponding to smooth, sand coated, and gear intruders, respectively.

The intruders are dropped or injected vertically by a "slingshot" consisting of a rubber band. We record images at 46 500 fps with a high-speed video camera (Photron FASTCAM SA5) that captures the impact process in detail, including the initial intruder speeds at impact. We determine the position of the intruder in each frame, as well as the force chain networks. The latter consists of photoelastic particles that appear bright in images, such as the typical examples in Fig. 1.

We use circular Hough transforms to locate and track the intruder position at each frame. We filter the position versus time data to avoid noise amplification and differentiate the trajectory to find the velocity [6,7]. We measure the angle of force chains at the boundary relative to the intruder radial direction. These angles provide information on the effective friction experienced by the intruder. If the networks are always parallel to the radial (normal) direction of the intruder (force chain angle $= 0$), then there is presumably little or no tangential force acting on the intruder. Deviations of the force chain directions from normal imply a tangential force. In previous experiments using smooth intruders, the force chains were found to be very close to normal, implying very weak effective friction. Here, we seek to understand what happens as the static friction of the intruder increases.

III. RESULTS AND DISCUSSIONS

Material responses in solid and liquid impact are relatively homogeneous and uniform. This is not the case in granular impact, where impact momentum is transferred via force chain networks and energy is dissipated by particle collisions and restitutional losses [5]. Figure 1 shows snapshots of force propagation for different intruders impacting on the photoelastic granular bed at similar initial impact speeds, near $v_0 \approx 2.2$ m/s. Figures 1(a) and 1(b) show force chains for the smooth and sandy intruders, respectively. As expected from the work of Clark *et al.*, the smooth intruder, which has a relatively low friction coefficient, $\mu = 0.37$, exhibits force chains that are along the radial direction at the intruder boundary. Likewise, for the sandy intruder, the force chains near the intruder boundary are oriented close to the intruder radial direction, even though the conventional friction coefficient of the sandy intruder, $\mu = 1.51$, is approximately four times that of the smooth one (see the video in the Supplemental Material [20]). However, the force chains generated by the gear intruder can penetrate into the granular bed in nonradial directions, including vertically into the bed when the radial and vertical directions differ substantially. Thus, the geometric friction caused by roughness at the size of the particles for the gear intruder is the key factor that changes the force chain directions. In turn, this increases the collisional drag force that opposes the intruder motion.

An additional factor affecting the geometric friction is the fact that the spacing between teeth of the gear intruder is very close to the diameter of the photoelastic particles. A row of particles is often entrained between the teeth. Consequently, the effective local intruder normal, which is set by the entrained grains, can be vertical, even though the mean normal direction, if the teeth were not present, is radial.

Figure 2(a) shows trajectories of the three intruders with similar initial impact speeds ($v_0 \approx 2.2$ m/s). The trajectories of the smooth and sandy intruders are nearly identical, while the gear intruder follows a different trajectory, with visibly shallower impact depth. The inset of Fig. 2(a) shows the depth differences vs time after impact between pairs of the three intruders during impact. The depth difference between smooth and sandy intruders (blue $\cdot$) is small and fluctuates near zero. In contrast, the depth difference between smooth or sandy intruders and the gear intruder increases roughly linearly. We also probed the dynamic differences of these intruders by examining the impact speeds and speed differences, as shown in Fig. 2(b). The difference between the smooth and sandy intruders is zero within the noise. The speed differences between smooth or sandy intruders and the gear intruder is initially nearly zero at impact and then grow to values of 0.1–0.2 m/s (with fluctuations) before falling back to zero when all the intruders have come to rest.

We plot the final depth z_{stop} vs $K_0 = \frac{1}{2}mv_o^2$ (m is the mass of intruder, and v_o is the speed at impact), shown in

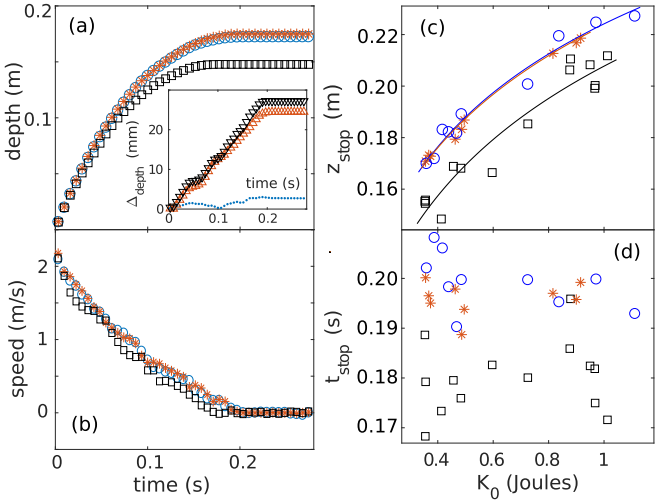

FIG. 2. (a) Intruder trajectories for for three different friction coefficient intruders with similar initial impact speeds, where $v_0 \approx 2.2$ m/s (○, smooth intruder; ∗, sandy intruder; and □, gear intruder). Inset: the differences of impact depth during impacting (·, the depth difference between smooth and sandy intruders; ∇, the depth difference between sandy and gear intruders; and △, the depth difference between smooth and gear intruders). (b) Impact speeds vs time. Here, $t = 0$ of (a) and (b) is the first contact with the granular surface, measured from the photoelastic response. (c) Final impact depth z_{stop} vs initial impact energy K_0 (blue line is the fitting curve for smooth intruder, with $a = 52.7$, $b = 55.4$, and $c = 10.0$; orange line is the fitting curve for sandy intruder, with $a = 54.4$, $b = 52.4$, and $c = 10.1$; black line is the fitting curve for gear intruder, with $a = 59.6$, $b = 29.8$, $c = 10.2$). (d) Total impact times with the different K_0.

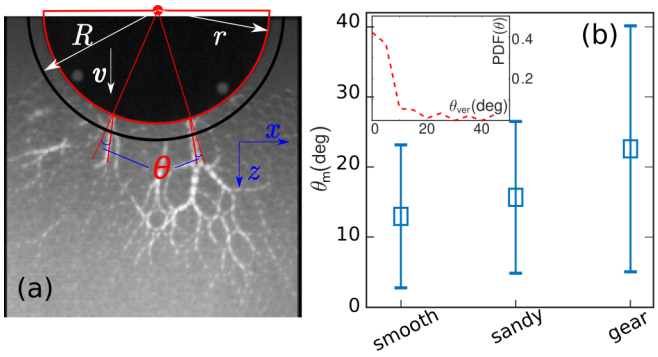

FIG. 3. (a) Schematic of the definition of θ, which is the angle between force chain segment contacting the surface of the intruder and the extension of the radial direction. r is the intruder radius, R corresponds to two particle diameters plus the intruder radius, which is used to characterize *forces chain around intruder*, v is the direction of gravity. (b) The mean value of θ generated by three different intruders. Inset: the probability distribution function of the force chain relative to the vertical direction θ_{ver} for gear intruder.

Fig. 2(c). z_{stop} and K_0 can be fitted by $z_{\text{stop}} = a\ln(bK_0 + 1) + c$ as described in [6]. Here, we focus on the differences among the three intruders only. We find that the smooth and sandy intruders with the same K_0 penetrate a similar depth. However, the final impact depth of the gear intruder at the same K_0 is consistently shallower than the smooth and sandy intruders, which means the kinetic energy of the gear intruder is dissipated faster during impacting. The total impact time of the gear intruder is also shorter, while the smooth and sandy intruders have very similar total impact times, as shown in Fig. 2(d).

We make two remarks on the penetration depth affected by intruder friction. First, the weak dependence of z_{stop} on intruder friction indicates that the drag force during impact is weakly affected by this friction. By contrast, Liao *et al.* reported that a rougher intruder would experience larger drag forces in the Brazil nut effect [21]. We attribute the absence of this effect of intruder roughness to different regimes of speed: the maximum speed in [21] was no more than 0.4 m/s, while the minimum initial impact speed in experiments here is approximately 2.2 m/s. Second, entrained particles might increase the effect intruder diameter by about 5%. The slight increase in the intruder diameter has been shown to have little effect on the penetration depth by Clark and Behringer [6]. In the case of gear intruder, particles that are picked up by intruder cusps at speed 0 m/s effectively reduce the impact kinetic energy, which may reduce the penetration depth. Therefore, the shorter penetration depth for the gear intruder is more likely caused by the geometric constraints.

Each intruder generates anisotropic force networks upon impact into the granular bed, which are captured using the photoelasticity of grains. For a low friction intruder, the force chains around it would, on average, extend radially outward, owing to the circular geometry of the intruder. In our case, the angle θ between force chains around the intruder and a reference radial direction [in Fig. 3(a)] provides the deviation from the frictionless case, and an indication of the effect of intruder friction on impact dynamics. Here, we only consider the magnitudes of θ.

Figure 3(b) shows mean values of θ generated by three different intruders with similar initial impact speed, where $v_0 \approx 2.2$ m/s. The force chains generated by sandy and smooth intruders were aligned closely to the local radial direction during impact (see the video in the Supplemental Material [20]), where the mean values of θ are only 12.97° and 15.68°, respectively. The effective friction coefficients, μ_* ($\mu_* = \tan\theta_m$), are 0.21 and 0.27, even though the friction coefficients between photoelastic particles and smooth and sandy intruders are 0.37 and 1.51, respectively. However, for the gear intruder, the angle of the force chains is generally not aligned with the intruder radial direction that would exist if there were no teeth. Rather, the force chains tend to penetrate into the granular bed vertically. Vertically oriented force chains occur when the particles become locked into the openings between the teeth. The inset of Fig. 3(b) shows the probability distribution function of the force chain relative to the vertical direction θ_{ver} for the gear intruder. The distribution shows most of the force chains generated by the gear intruder have a very small angle (less than 10°) relative to the vertical direction. The θ_m ($\theta_m = 22.6°$) for the gear intruder is clearly higher than that for the smooth and sandy intruders, and corresponds to effective friction coefficient $\mu_* = 0.42$. Meanwhile, the standard deviation $\delta\theta$ for the three different intruders is also different. The value of $\delta\theta$ ($\delta\theta = 18°$) for the gear intruder is nearly twice that of the smooth ($\delta\theta = 10°$)

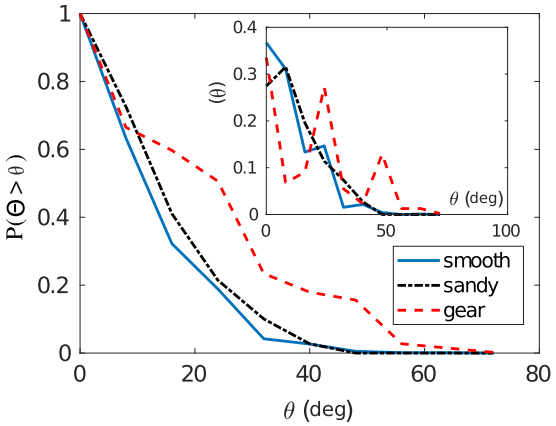

FIG. 4. The cumulative distribution function $P(\Theta > \theta)$ for the three different intruders vs the angle between interface force chains and the reference radial direction θ, with the initial kinetic energy $K_0 = 0.4J$ for all of three intruders. Inset: The probability distribution function $P(\theta)$ for the three different intruders vs θ.

and sandy ($\delta\theta = 11^\circ$) intruders, which indicates that the gear intruder generates large angle force chains, relative to the intruder surface.

In order to understand the behavior of the mean and standard deviation of θ, we investigate the probability distribution function (PDF) $P(\theta)$ and cumulative distribution function (CDF) $P(\Theta > \theta)$. Figure 4 (main) shows the cumulative distribution functions $P(\Theta > \theta)$, calculated by integrating $P(x)$ over x from θ to the maximum observed angle, slightly smaller than 80°. This distribution shows a significant difference between the gear intruder and the smooth and sandy intruders for $\theta >\sim 10^\circ$. There are many more frictional contacts associated with geometrical interlocking between gears and grains, which evidently affects the impact dynamics, as shown previously in Fig. 2. This observation suggests that using geometrical asperities as a model for friction [19], while effective in generating static structures, may introduce unintended results in the dynamical regime.

For $P(\theta)$, Fig. 4 (inset), the difference between the gear intruder and the smooth and sandy intruders is also clear. There are two notable points: first, $P(\theta)$ is much higher at large θ in the gear intruder case than the other two; and second, $P(\theta)$ shows several peaks for the gear intruder; in comparison, $P(\theta)$ is fairly smooth for the other two cases. The peaks in $P(\theta)$ for the gear intruder are likely due to the complex surface structure associated with the outward pointing edges of the gears and the tendency of grains to become trapped in the gears, leading to a complex surface.

IV. CONCLUSIONS

To conclude, the friction in granular impact can be categorized into friction associated with small scale and grain-scale roughness. Significant differences in the small scale roughness, associated with conventional frictional coefficients, have a limited effect on granular impact dynamics. But roughness at the grain scale, leading to geometric friction, causes substantially different force chain dynamics at the intruder boundary, and consequently different drag on the intruder. The geometric friction means that the roughness level of the intruder has to be able to trap at least one particle. Results for intruders with small scale roughness validate the assumption used in a recent collision model for the drag force [7] of normal collisions with the force chains and minimal friction. The difference between small scale and geometry friction is evident in macroscopic properties such as the impact time and the penetration depth. A detailed investigation of an angle θ, characterizing the deviation of force chain orientation from the intruder's radial direction at the contact point, shows there are more contributions from force chains at much larger θ during impact in the case of geometry friction than that of the conventional friction.

ACKNOWLEDGMENTS

We are grateful to C. Bester and J. Dijksman for their assistance. This work was supported by NSFC Grant No. 41672256(HZ), NSF Grant No. DMR1206351, NASA Grant No. NNX15AD38G, the William M. Keck Foundation, and a RT-MRSEC fellowship.

[1] W. Kang, Y. Feng, C. Liu, and R. Blumenfeld, Nat. Commun. **9**, 1101 (2018).
[2] L. A. López-Rodríguez and F. Pacheco-Vázquez, Phys. Rev. E **96**, 030901 (2017).
[3] W. A. Allen, E. B. Mayfield, and H. L. Morrison, J. Appl. Phys. **28**, 370 (1957).
[4] H. Katsuragi and D. Durian, Nat. Phys. **3**, 420 (2007).
[5] A. H. Clark, L. Kondic, and R. P. Behringer, Phys. Rev. Lett. **109**, 238302 (2012).
[6] A. H. Clark and R. P. Behringer, Europhys. Lett. **101**, 64001 (2013).
[7] A. H. Clark, A. J. Petersen, and R. P. Behringer, Phys. Rev. E **89**, 012201 (2014).
[8] M. P. Ciamarra, A. H. Lara, A. T. Lee, D. I. Goldman, I. Vishik, and H. L. Swinney, Phys. Rev. Lett. **92**, 194301 (2004).
[9] Y. Takehara and K. Okumura, Phys. Rev. Lett. **112**, 148001 (2014).
[10] H. Zheng, D. Wang, J. Barés, and R. P. Behringer, Phys. Rev. E **98**, 010901 (2018).
[11] M. X. Lim and R. P. Behringer, Europhys. Lett. **120**, 44003 (2018).
[12] T. Børvik, S. Dey, and L. Olovsson, Int. J. Impact Eng. **75**, 123 (2015).
[13] A. Seguin, Y. Bertho, P. Gondret, and J. Crassous, Phys. Rev. Lett. **107**, 048001 (2011).
[14] A. Seguin, Y. Bertho, F. Martinez, J. Crassous, and P. Gondret, Phys. Rev. E **87**, 012201 (2013).
[15] T. A. Brzinski III, J. Schug, K. Mao, and D. J. Durian, Phys. Rev. E **91**, 022202 (2015).
[16] S. P. D. Birch, M. Manga, B. Delbridge, and M. Chamberlain, Phys. Rev. E **90**, 032208 (2014).

[17] C. S. Bester and R. P. Behringer, Phys. Rev. E **95**, 032906 (2017).
[18] A. H. Clark IV, Ph.D. thesis, Duke University, 2014.
[19] S. Papanikolaou, C. S. O'Hern, and M. D. Shattuck, Phys. Rev. Lett. **110**, 198002 (2013).
[20] See Supplemental Material at http://link.aps.org/supplemental/10.1103/PhysRevE.98.032904 for additional information on force chain network dynamics in front of intruders.
[21] C.-C. Liao, S.-S. Hsiau, and C.-S. Wu, Phys. Rev. E **86**, 061316 (2012).